IEEE Access
Multidisciplinary | Rapid Review | Open Access Journal

Received July 13, 2020, accepted July 24, 2020, date of publication July 30, 2020, date of current version August 11, 2020.

Digital Object Identifier 10.1109/ACCESS.2020.3012994

Substrate Integrated Waveguide Bandpass Filtering With Fourier-Varying Via-Hole Walling

OSAMA I. HUSSEIN[1], (Student Member, IEEE), KHAIR A. AL SHAMAILEH[2], (Member, IEEE), NIHAD I. DIB[3], (Senior Member, IEEE), AMIR NOSRATI[4], SAID ABUSHAMLEH[5], (Member, IEEE), DANIEL G. GEORGIEV[1], (Senior Member, IEEE), AND VIJAY KUMAR DEVABHAKTUNI[2], (Senior Member, IEEE)

[1]Electrical Engineering and Computer Science Department, The University of Toledo, Toledo, OH 43606, USA
[2]Electrical and Computer Engineering Department, Purdue University Northwest, Hammond, IN 46322, USA
[3]Electrical Engineering Department, Jordan University of Science and Technology, Irbid 22110, Jordan
[4]School of Electrical and Computer Engineering, University of Tehran, Tehran 14174661191, Iran
[5]Physics Department, The University of Nebraska at Kearney, Kearney, NE 68849, USA

Corresponding author: Khair A. Al Shamaileh (kalshama@pnw.edu)

ABSTRACT In this article, an optimization-driven methodology is proposed for the design of substrate integrated waveguide (SIW) bandpass filters (BPFs) with predefined passbands. The width between the metallic walls of via-holes is governed by a truncated Fourier series to achieve the desired filtering performance. The theory of rectangular waveguide is used to establish the optimization framework and obtain the series coefficients under predefined physical constraints. Two types of end-terminations are studied; specifically, with and without SIW-to-microstrip transitions. To validate the proposed methodology, two Ku-band BPF prototypes with 2.5% and 5.8% 15-dB fractional bandwidth (FBW) are designed, simulated, and measured. Furthermore, the half-mode SIW (HMSIW) concept is incorporated in one prototype to facilitate a miniaturized physical structure. Simulations and measurements are in close proximity with passband matching and transmission losses better than –15 dB and –2.5 dB, respectively. The proposed methodology allows for designing BPFs with predefined wideband or narrowband FBW by modifying the underlying physical constraints and optimization parameters. The resulting filters are planar, compact, and have wide stopband rejection. In addition, a derivation for the characteristic impedance of the SIW line is provided, which can be used to find the optimum SIW-to-microstrip transition without performing a parametric study.

INDEX TERMS Bandpass filter (BPF), half-mode substrate integrated waveguide (HMSIW), SIW-to-microstrip transition, narrowband, rectangular waveguide, substrate integrated waveguide (SIW), wideband.

I. INTRODUCTION

Substrate integrated waveguide (SIW) technology has attracted a significant attention lately due to its excellent electrical performance at the millimeter wave range. In addition, this technology intertwines the advantages of rectangular waveguides and planar circuits, such as the high Q-factor, low radiation losses, light-weight, and ease of fabrication. Therefore, SIW is widely utilized in millimeter wave front-end subsystems.

Bandpass filters (BPFs) are widely used in modern millimeter wave circuitry [1]–[4]. Consequently, efforts have been devoted towards developing BPFs with improved electrical properties (e.g., low passband losses) without compromising the physical features (e.g., structural dimensions). SIW-based BPFs, in particular, have attracted a special attention for their contribution in eliminating unwanted transverse-magnetic propagation modes and out-of-band parasitic responses [5]. To this end, a multitude of SIW and half-mode SIW (HMSIW) based BPF layouts were introduced, all of which demonstrated an excellent performance [6]–[18]. In [6], a hybrid spoof surface plasmon polariton was adopted in the design of a broadband SIW filter. However, the associated structural complexity and stopband characteristics setback its ready acceptance. Cavities and resonators were used to realize BPFs with transmission zeros and improved selectivity [7]–[13]. Nevertheless, the resulting physical area, high insertion losses and/or poor stopband

The associate editor coordinating the review of this manuscript and approving it for publication was Andrei Muller.

rejection were major drawbacks. A trisection filter with a frequency-dependent cross-coupling was proposed in [14]. However, frequency matching was achieved at the expense of the stopband rejection level and passband insertion loss. A folded SIW filter using high permittivity ceramic substrates was proposed in [15]. While this approach promises a compact design and temperature stability, fabrication complexity and unsuitability to high-frequency applications are major disadvantages that potentially limit its adoption in high-frequency applications.

The HMSIW technology combined with Koch fractal shape electromagnetic bandgap (EBG) structures and co-planar waveguide resonators were recently introduced to miniaturize the overall filter area [16], [17]. In addition, quarter- and eighth-mode SIW cavities are used to design BPFs in [18]. Nevertheless, such multilayer designs come at the cost of increased fabrication precision.

In this article, the via-hole walling in a conventional SIW layout is varied based on a truncated Fourier series as shown in Fig. 1 to obtain bandpass filtering characteristics.

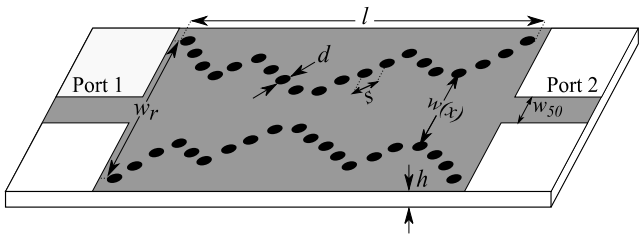

FIGURE 1. A schematic diagram of the proposed SIW-based BPF structure with varying via-hole walling without SIW-to-microstrip transition. White, grey and black colors represent the substrate, metal and via-holes, respectively.

The proposed method has the following features: 1) the fractional bandwidth (FBW) is defined by modifying the optimization parameters, 2) stopband rejection levels are obtained without incorporating higher-order modes of SIW cavities, and 3) compactness is achieved through optimized structural dimensions with or without SIW-to-microstrip transitions (e.g., tapered lines).

This article is organized as follows: the design methodology and mathematical guidelines of the proposed SIW-based BPFs with varying via-hole walling are presented in Section II. Simulations and measurements for different passband examples are given in Section III. Finally, conclusions are drawn in Section IV.

II. DESIGN METHODOLOGY

It was found that an SIW structure has the same dispersion characteristics of a rectangular waveguide filled with the same substrate material provided that an effective width, w_{eff}, is used instead of its actual width, w [19]. It is also well-known that conventional rectangular waveguides have a highpass response above the cutoff frequency. Thus, another higher cutoff frequency is required to achieve a bandpass operation. The common techniques that serve for this purpose are based on cavities, resonators, or EBGs. However, this comes at the cost of higher passband losses and/or larger physical area. In this work, the cutoff frequencies are controlled by varying the SIW width (i.e., varying the locations of the via-holes).

In this section, the design methodology of the varying via-hole walling BPFs is elaborated. Sub-section II.A presents the design methodology without considering matching networks; whereas the design guideline taking into account matching networks (i.e., Klopfenstein tapered microstrip-to-SIW transition) is given in II.B. Fig. 2 illustrates the effect of the matching networks on a conventional SIW structure. In contrast to the case where no matching networks are used, an SIW with a tapered transition results in a highpass response. This work aims to achieve bandpass filtering in both cases.

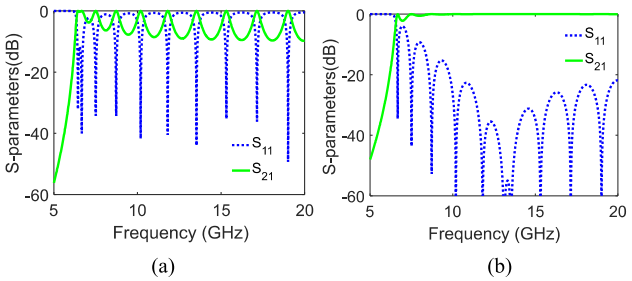

FIGURE 2. S-parameters of a conventional SIW structure: (a) without matching networks, and (b) with a tapered SIW-to-microstrip transition.

A. FILTER DESIGN WITHOUT MATCHING NETWORKS

According to Fig. 1, no matching network is incorporated in the SIW structure in order to reduce the overall filter dimensions. As mentioned earlier, it is possible to adopt the theory of rectangular waveguides in SIW configurations provided that w_{eff} is used instead of w. To this end, different empirical formulas were proposed to calculate w_{eff} [20]–[22]. In this article, the following expression is used for its accuracy in modeling the various SIW parameters [22]:

$$w_{eff} = w - 1.08\frac{d^2}{s} + 0.1\frac{d^2}{w} \tag{1}$$

where w is the width between the rows of via-holes in a conventional SIW layout, d is the diameter of the via-hole, and s is the Euclidean distance between any two adjacent via-holes. The expression in (1) is valid for $s/d < 3$ and $d/w < 0.2$ to avoid leakage losses between the via-holes [22]. In this work, the width between the metallic walls (i.e., via-hole locations) is varied to obtain predefined electrical properties under physical constraints including ports matching and machining tolerance. The cutoff frequency, f_c, of the dominant mode in an SIW structure is inversely proportional to w_{eff}, and is given as:

$$f_c = \frac{c}{2w_{eff}\sqrt{\varepsilon_r}} \tag{2}$$

where c is the speed of light and ε_r is the relative substrate permittivity. Therefore, varying the width (i.e., w_{eff}) leads to variations in f_c. Consequently, the upper and lower cutoff

frequencies of an SIW-based BPF are achieved by optimizing the width pattern as will be explained later in greater details.

The analysis begins by subdividing the effective width, $w_{eff}(x)$, into M uniform segments, each of a length $\Delta x = l/M$, where l is a predefined length chosen to realize a compact layout. M is chosen such that $\Delta x \ll \lambda_g$, where λ_g is the guided wavelength at the center frequency of the design bandwidth. Fig. 3 shows the variations of w_{eff} and f_c at the center of each segment $\Delta x_m = [m–0.5]\Delta x$ $(m = 1,2, \ldots M)$ versus the physical length of the SIW structure. In this example, M and l are set to 20 and 20 mm, respectively. It can be observed that some segments have a cutoff frequency below the passband (i.e., propagation mode); whereas others have a cutoff frequency higher than the passband (i.e., evanescent mode). These variations in f_c lead to the desired BPF response. The analysis continues by modeling $w_{eff}(x)$ in a truncated Fourier series in the form [23]:

$$w_{eff}(x) = w_r \exp\left[\sum_{n=0}^{N} a_n \cos\frac{2\pi n x}{l}\right] \tag{3}$$

where N is the number of the series coefficients and w_r is a reference effective width, which is obtained based on f_c [22]. The resulting $w_{eff}(x)$ should adhere to reasonable fabrication limitations and matching conditions. That is:

$$w_{min} \le w_{eff}(x) \le w_r \tag{4.a}$$
$$w_{eff}(0) = w_{eff}(l) = w_r \tag{4.b}$$

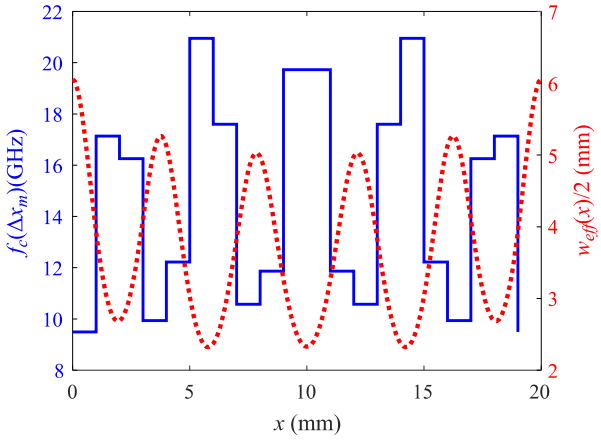

FIGURE 3. Cutoff frequency/width variations at the center of each SIW segment versus length. Solid blue and dotted red represent f_c and $w_{eff}(x)/2$, respectively.

The constraint in (4.a) limits the variation of $w_{eff}(x)$ within a maximum value $w_{max} = w_r$ and a minimum value $w_{min} = 5d$ to satisfy the conditions imposed by (1); whereas the constraint in (4.b) enforces equal widths at both ends of the SIW structure, and is realized by satisfying the following condition:

$$\sum_{n=0}^{N} a_n = 0 \tag{5}$$

In order to apply transmission-line theory to rectangular waveguide, the phase constant, β, and the characteristic impedance, Z_0, should be calculated for each segment. Taking into account the dominant mode, β is obtained as follows [24]:

$$\beta(\Delta x_m) = \sqrt{\omega^2\mu\varepsilon - \left(\frac{\pi}{w_{eff}(\Delta x_m)}\right)^2} \tag{6}$$

where ω is the radian frequency, μ is the permeability, and ε is the permittivity. On the other hand, there is no unique definition for the waveguide characteristic impedance. Rather, existing definitions differ by a constant k [25]. To find this constant, the power-current definition is used initially, which is given as [25]:

$$Z_{0,pi}(\Delta x_m) = k\frac{h}{w_{eff}(\Delta x_m)}\sqrt{\frac{\mu_r}{\varepsilon_r}}\frac{\lambda_g(\Delta x_m)}{\lambda} \tag{7}$$

where h is the substrate thickness, $k = 465$, and λ_g/λ is given as:

$$\frac{\lambda_g(\Delta x_m)}{\lambda} = \frac{1}{\sqrt{1-(f_c(\Delta x_m)/f)^2}} \tag{8}$$

With the aforementioned k value, it is found that there is a discrepancy between the simulated characteristic impedance and $Z_{0,pi}$ obtained from (7). This discrepancy is more significant around the cutoff frequency. Moreover, the change in some design parameters (e.g., w_{eff}, ε_r, h) necessitates a different constant to achieve the best agreement between the analytical and simulated/measured responses. Accordingly, (7) is modified to the following form (derivation is provided in Appendix 1):

$$Z_0(\Delta x_m) = k'\frac{h}{w_{eff}(\Delta x_m)}Z_{wave}(\Delta x_m) \tag{9}$$

where $Z_{wave}(\Delta x_m) = \omega\mu/\beta(\Delta x_m)$. The value of k' is selected such that the calculated and simulated waveguide characteristic impedances are equivalent. The characteristic impedance in (7) and (9) are plotted in Fig. 4 together with the simulated impedance from ANSYS Electronics Desktop [26] for different w_{eff} and h values considering $\varepsilon_r = 3.55$. The accuracy of (9) outperforms that obtained from (7), which validates its

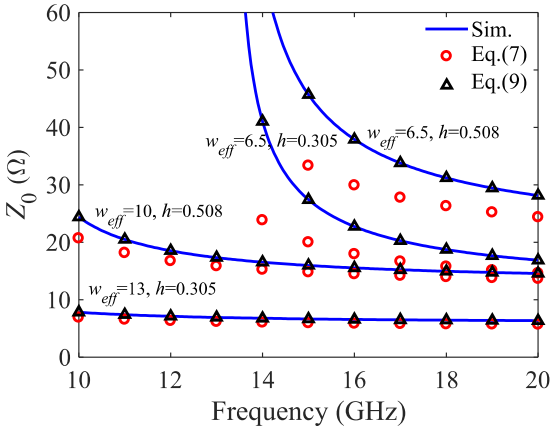

FIGURE 4. Simulated versus analytical Z_0 based on (7) and (9) plotted for different w_{eff} and h (units in mm).

use in the proposed methodology. Once Z_0 is evaluated for all M segments, the $ABCD$ parameters of the m^{th} segment are obtained as follows:

$$A_m = D_m = \cos\left[\Delta x.\beta\left(\Delta x_m\right)\right] \tag{10.a}$$

$$B_m = Z_0^2\left(\Delta x_m\right) C_m = jZ_0\left(\Delta x_m\right)\sin\left[\Delta x.\beta\left(\Delta x_m\right)\right] \tag{10.b}$$

Then, the $ABCD$ matrix of the SIW structure is found by multiplying the $ABCD$ matrices of all M segments as follows:

$$[AB;\, CD] = \prod_{m=1}^{M} [AB;\, CD]_m \tag{11}$$

The resulting overall $ABCD$ matrix is used to express the input port matching, S_{11}, and the transmission parameter, S_{21}, of the SIW-based structure, which are given as follows [24]:

$$S_{11} = \frac{AZ_{\mu s} + B - CZ_{\mu s}^2 - DZ_{\mu s}}{AZ_{\mu s} + B + CZ_{\mu s}^2 + DZ_{\mu s}} \tag{12.a}$$

$$S_{21} = \frac{2(AD - BC)Z_{\mu s}}{AZ_{\mu s} + B + CZ_{\mu s}^2 + DZ_{\mu s}} \tag{12.b}$$

where $Z_{\mu s} = 50\text{-}\Omega$ is the characteristic impedance of the microstrip feedline. Once the S-parameters are expressed in terms of the $ABCD$ matrix of the SIW structure, the following error function is established for a bandpass filtering response:

$$E = \begin{cases} \sqrt{(|S_{11}| - 1)^2 + \alpha|S_{21}|^2}, & f_{min} \le f \le f_{cL} \\ & f_{cH} \le f \le f_{max} \\ \sqrt{\alpha|S_{11}|^2 + (|S_{21}| - 1)^2}, & f_{cL} \le f \le f_{cH} \end{cases} \tag{13}$$

where f_{cL} and f_{cH} are the lower and higher cutoff frequencies of the passband, respectively, and α is a weighting factor used to minimize the reflection coefficient in the passband and increase the lower/higher rejection levels in the stopband. The error vector resulting from applying (13) to all frequency points within $[f_{min}, f_{max}]$ is used to establish the following objective function:

$$\text{Objective} = \sqrt{\frac{1}{M_f}\sum_{i=0}^{M_f} E\left(f_{\min} + i\Delta f\right)} \tag{14}$$

where $M_f = (f_{max} - f_{min})/\Delta f + 1$ is the number of frequency points and $\Delta f = 0.05$ GHz is a frequency increment. The Fourier coefficients, a_n, that result in an optimum bandpass filtering response are found by minimizing (14). The genetic algorithm (GA) is used in this context for its applications in microwave and millimeter-wave front-ends design and optimizations [27]–[30]. Table 1 illustrates the adopted optimization settings. It is noteworthy to point out that there is no unique solution for the coefficients (i.e., different a_n's in each run). Therefore, the coefficients with the optimal response, in combination with a width profile $w_{eff}(x)$ that satisfies (4) is considered in the following design steps. The separation between the centers of the via-holes, s, is calculated based on the Euclidean distance.

TABLE 1. List of optimization parameters.

GA Parameter	Value
No. of generations	700
Population size	200
Crossover rate	0.7
Mutation rate	0.1
Series coefficients	$\in\{-1,1\}$
Function tolerance	1×10^{-20}

Algorithm 1 shows a pseudocode of the proposed Fourier-varying via-hole BPF. Three examples are optimized based on the outlined analysis considering a 0.3048-mm-thick Rogers RO4003C substrate with $\varepsilon_r = 3.55$. The physical dimensions of these filters are listed in Table 2. The three designs have a center frequency of 14 GHz and FBWs of 2.5%, 5.8%, and 18.2%. The number of the series coefficients, N, and the uniform segments, M, are set to 7 and 80, respectively. Finally, k' is set to 1.265; whereas α is chosen to be 30.

TABLE 2. List of physical dimensions of The SIW BPFs.

Parameter	Value (mm)	Parameter	Value (mm)
d	0.50	w_{min}	2.50
s	0.90	l	40.0
$w(x{=}0,l)$	13.0	w_{50}	0.68
$w_r = w_{max}$	12.7		

Fig. 5 illustrates the analytical results of the three designs, which all show input port matching better than –20 dB and passband transmission better than –0.2 dB. Fig. 6 shows the width profiles of the three design examples, which are

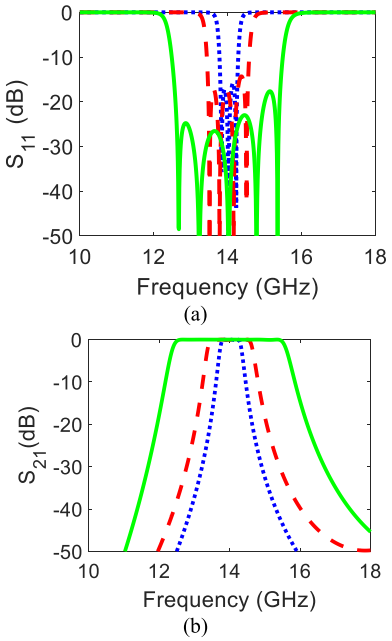

FIGURE 5. Analytical results of three SIW BPFs with different passbands. Blue dotted, red dashed, and green solid lines represent passbands of 13.8–14.2 GHz, 13.5–14.5 GHz, and 12.5–15.5 GHz, respectively.

Algorithm 1 Fourier-Varying Via-Hole Walling SIW BPF Design

Input: $[\varepsilon_r, h]$ - Substrate Parameters;
$[d, s, w(0), l]$ - Filter Physical Dimensions;
$[w_{\min}, w_{\max}]$ - Width Constraints;
$[f_{cL}, f_{cH}]$ - Lower/Higher Passband Frequencies;
$[f_{min}, f_{max}, \Delta f]$ - Frequency Range and Step;
$Z_{\mu s}$ - Microstrip Port Impedance;
M - No. of Uniform Segments;
N - No. of Fourier Series Terms;
$[k', \alpha]$- Constants;

1: Procedure E_wall_varied_SIW_BPF()
2: $w_r \leftarrow$ **Effective_Width**$(w(0), d, s)$;
3: ***Loop:*** **for each frequency do**
4: **for each** m **segment do**
5: $w_{eff}(\Delta x_m) \leftarrow$ Varied_Width $(w_r, a_n, \Delta x_m, l, N)$;
// Δx_m represents the center of the m^{th} segment
// initial coefficients, a_n, are assumed
6: $\beta(\Delta x_m) \leftarrow$ Beta$(f, \varepsilon_r, w(\Delta x_m))$;
7: $Z_0(\Delta x_m) \leftarrow$ Charac_Imped $(k', h, w_{eff}(\Delta x_m), \beta(\Delta x_m), f)$;
8: $[AB;CD]_m \leftarrow ABCD$_Matrix$(l, M, \beta(\Delta x_m), Z_0(\Delta x_m))$;
9: $[AB;CD] \leftarrow$ Overall_ABCD_Matrix();
10: **end for**
11: $[S_{11}, S_{21}] \leftarrow S$-Parameters$([AB; CD], Z_{\mu s})$;
12: $[E] \leftarrow$ Set_Error_Value$([S_{11}, S_{21}], [f_{cL}, f_{cH}, f_{min}, f_{max}, \Delta f], \alpha)$;
13: **end for**
14: $[[a_0, \ldots, a_N]$,Objective$] \leftarrow$ Minimize_Sum_of_Errors$([E])$;
// a_n being the optimization variables
15: **Repeat** ***Loop*** **until optimal $[a_1, \ldots, a_N]$;**
// or predefined iterations
16: end Procedure

constrained by the predefined $w_{min,max}$. In addition, the end terminations of the three profiles equal w_r. Hence, the results of the three designs validate the proposed methodology.

B. FILTER DESIGN WITH KLOPFENSTEIN MATCHING NETWORK

In this section, Klopfenstein tapered lines are used to improve the passband response of the proposed filters [31]. The characteristic impedances at end-terminations, $Z_0(x = 0, l)$, are found using (9). Then, (12) is calculated, where $Z_{\mu s} = Z_0(x = 0, l)$. The Klopfenstein taper is expressed as [32], [33]:

$$\ln\left(\frac{Z(x)}{Z_s}\right) = 0.5 \ln\left(\frac{Z_l}{Z_s}\right)\left[1 + G\left(B, 2\left(\frac{x}{d_t} - 0.5\right)\right)\right] \quad (15)$$

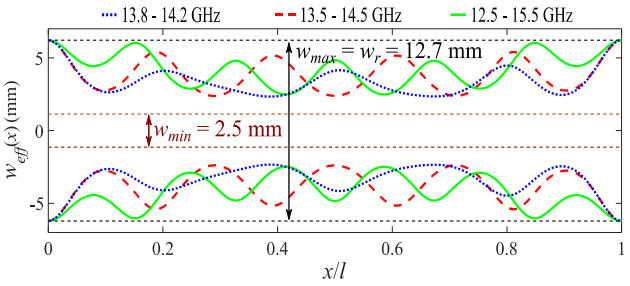

FIGURE 6. Width-varying profiles of the BPFs as a function of the normalized length.

where $Z_{s,l}$ represent the source and load impedances at the two ends of the tapered line (i.e., $Z_s = 50$-Ω, $Z_l = Z_{\mu s}$), and d_t is the taper length, and

$$G(B, \xi) = \frac{B}{\sinh B} \int_0^{\xi} I_0\left(B\sqrt{1 - \xi'^2}\right) d\xi' \quad (16)$$

where B is a predefined design parameter that determines the tapered profile and $I_0(x)$ represents the modified zero-order Bessel function. Higher B values improve the input matching at the expense of a longer taper. For a given taper line, the maximum input return loss (in dB) is given as [32], [33]:

$$\left|RL_{input}\right|_{\max} = -20 \log\left[\tanh\left(\frac{B}{\sinh B}\right)(0.21723) \ln\left(\sqrt{\frac{Z_l}{Z_s}}\right)\right] \quad (17)$$

A HMSIW filter configuration is also proposed with tapered lines to facilitate the necessary impedance matching as shown in Fig. 7. HMSIW is adopted to reduce the filter dimensions [34].

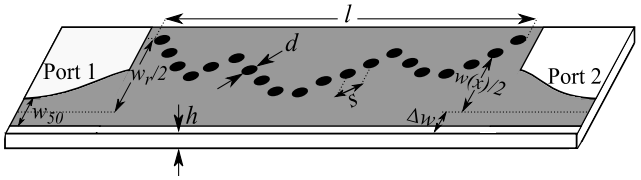

FIGURE 7. A schematic diagram of the proposed HMSIW filter with SIW-to-microstrip transitions and varying via-hole walling. White, grey and black colors represent the substrate, metal and via-holes, respectively.

For an optimum HMSIW operation, the substrate width should be increased slightly to mitigate the fringing effects. The necessary width increase is found empirically as follows [35]:

$$\Delta w = h \times \left(0.05 + \frac{0.3}{\varepsilon_r}\right) \times \ln\left(7.9 \times 10^{-4} \frac{w_r^2}{h^3} + \frac{0.104 w_r - 2.61 \times 10^{-4}}{h^2} + \frac{0.038}{h} + 2.77\right) \quad (18)$$

Then, the effective width of the HMSIW structure is given as:

$$w_{eff,HM}(x) = \frac{w_{eff}(x)}{2} + \Delta w \quad (19)$$

Since $w_{eff,HM} < w_{eff}$, $Z_{0,HM}$ is higher than Z_0 in the conventional SIW structure. Hence, for better matching, the transition width of the HMSIW filter, $w_{\mu s,HM}$, is approximately $w_{\mu s}/2$ [36].

III. SIMULATIONS AND MEASUREMENTS

In this section, simulations and measurements for three BPF prototypes are presented. Prototype (1) is optimized for a 5.8% FBW at 14 GHz center frequency following the procedure presented in Section II.A. Prototype (2) is interfaced with Klopfenstein tapered lines as discussed in Section II.B, and is optimized for a 2.5% FBW at 12 GHz center frequency. Finally, Prototype (3) demonstrates the HMSIW layout of prototype (2). It is noteworthy to mention that the optimization parameters and physical dimensions listed in Tables 1 and 2 are adopted in the three designed prototypes. ANSYS Electronics Desktop is used for simulations; whereas measurements are performed with Agilent E8362C network analyzer. Short-open-load-thru calibration is performed to the network analyzer ports with Keysight 3.5 mm mechanical calibration kit to shift the reference plane to the output of the coaxial cables. The fabrication is performed using the standard printed circuit board process with copper filled via-holes.

The simulated and measured S-parameters of prototype (1) and a photograph of the fabricated structure are shown in Fig. 8. The filter has passband port matching and transmission loss better than –15 dB and –2.5 dB, respectively. The maximum upper rejection level is better than –40 dB with a rejection better than –20 dB for 3 GHz after the operating band.

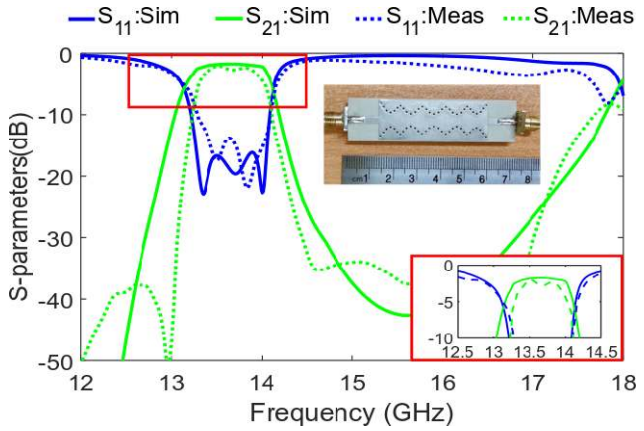

FIGURE 8. Simulations and measurement of the designed SIW-based BPF with a FBW of 5.8% and 14 GHz center frequency.

Similarly, the simulated and measured S-parameters of prototype (2) and a photograph of the fabricated structure are shown in Fig. 9. Here, a highly-selective narrowband filter is interfaced with tapered lines. The characteristic impedance in this example is found to be $Z_0 = 7.5$-Ω at the center frequency, which results in $w_{\mu s} = 7.46$ mm. The length of the tapered lines and the value of B are set to 10 mm and 2.5,

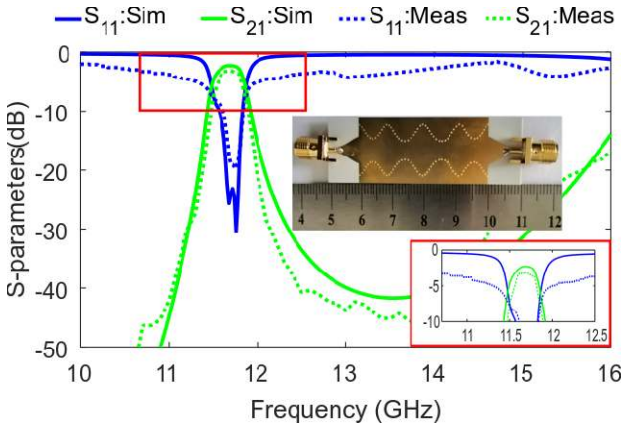

FIGURE 9. Simulations and measurement of the designed SIW-based BPF with a FBW of 2.5% and 12 GHz center frequency.

respectively. Here, passband input port matching and transmission loss better than –19 dB and –3.0 dB, respectively, are obtained.

Finally, the simulated and measured S-parameters of prototype (3) and a photograph of the fabricated structure are shown in Fig. 10. Simulations and measurements are in good agreement. Both the SIW and HMSIW filters have the same order. However, the latter has a slightly broader bandwidth and lower stopband rejection level due to power leakage from the open side aperture in the HMSIW layout, resulting in higher radiation losses near the cutoff frequency [35]. Discrepancies between the simulated and measured results in all prototypes, including the shift in the center frequency, are attributed to the fabrication tolerance, SMA connectors, as well as substrate permittivity and thickness tolerances.

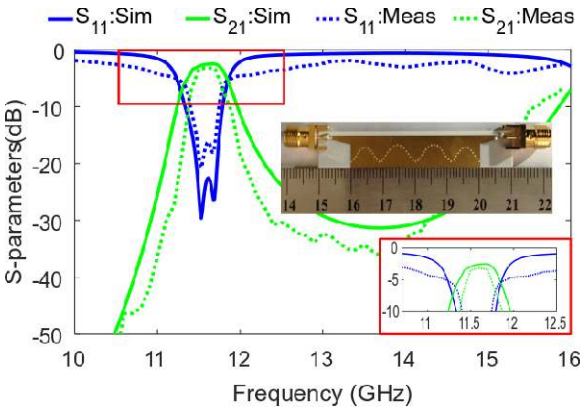

FIGURE 10. Simulations and measurements of the designed HMSIW-based BPF with a FBW of 2.5% and 12 GHz center frequency.

Table 3 shows the optimized series coefficients and the value of (14) for the three prototypes. Table 4 represents a comparison between the proposed methodology and other state-of-the-art techniques. The proposed method shows acceptable electrical characteristics as compared to other reported efforts. It is worth mentioning that narrowband filters impose higher insertion losses as observed in

TABLE 3. Optimized fourier series coefficients and the corresponding error.

		a_0	a_1	a_2	a_3	a_4	a_5	a_6	Value of (14)
Prototype (1)	(FBW: 5.8%)	–0.5082	0. 0869	0. 0417	0.0178	0.0671	0. 3733	0.0656	0.6342
Prototypes (2&3)	(FBW: 2.5%)	–0.4675	0.0818	0.0311	–0.1765	0.4233	0.0955	0.0125	0.4833

TABLE 4. Comparison between the Proposed BPFs and other State-of-the-art SIW BPFs.

Ref.		Applied Technique	Center Freq. (GHz)	FBW (%)	Return Loss (dB)	Insertion Loss (dB)	Stopband BW with rejection > 20 (GHz)	Area* (λ_g^2)
[7]		Four side-by-side SIW cavities with one cross-coupling	10.00	1.2	14.0	3.90	0.30	2.1
[11]		Transversal filter using modified-doublet with non-coupled resonators	14.87	0.9	14.3	4.20	3.00	4.4
[12]		Higher-order resonators with modified feeding and bypass coupling topology	8.25	1.2	15.0	3.32	2.25	4.0
[13]		Modified trisection topology with planar microstrip resonators	5.10	4.2	18.0	2.50	1.00	1.52
[14]		Triplet configuration with frequency-dependent cross-coupling	4.85	3.7	17.8	5.00	0.6	2.9
[16]		HMSIW filter with Koch fractal EBG etched on the top plane	3.40	25.0	11.4	1.70	2.30	0.45
This Work	Prototype (1)	E-wall-varied SIW filter without SIW-to-microstrip transition	13.70	5.8	15.0	2.50	3.00	2.94
	Prototype (2)	E-wall-varied SIW filter with SIW-to-microstrip transition	11.70	2.5	19.0	3.00	3.75	1.96
	Prototype (3)	E-wall-varied HMSIW filter with SIW-to-microstrip transition	11.65	2.5	16.0	3.30	2.95	1.04

* Feedlines are not included in the calculation of the occupied area

prototypes 2 and 3 [12]. Specifically, designing BPFs with FBW less than 5% is challenging due to the associated increase in the insertion loss [37]. Thus, the proposed filters have lower loss than other reported efforts except [13] and [16], which have higher FBWs and lower center frequencies. This method offers flexibility in FBW redefinition without extra components (e.g., resonators, EBG).

The proposed methodology differs from other previous efforts in the following aspects: 1) Unlike [7], [11], [12], and [14], all BPF designs presented in this work occupy smaller area and has lower insertion losses due to the absence of higher-order modes of cavities and resonators. 2) In contrast to the multilayer filters elaborated in [8], [18], the resulting filter designs in this work are planar and implemented on a single layer substrate. 3) Although the use of microstrip resonators instead of SIW cavities in [13] contributed a miniaturized circuit area, such resonators may introduce additional losses at higher frequencies; thus, limiting their use in high-frequency applications.

IV. CONCLUSION

A systematic methodology is proposed for the design of planar BPFs based on varied SIW and HMSIW via-hole walling governed by a truncated Fourier series expansion. The optimized locations of the via-holes allow predefined bandwidth and acceptable electrical performance. For verification, three prototypes are simulated, fabricated and measured. Simulated and measured results are in a good agreement in both pass- and stop-bands. Differences between simulated and measured results are attributed mainly to the fabrication process and substrate parameters.

The proposed method allows the design of narrowband or wideband BPFs by modifying the optimization parameters. In addition, the proposed method can be utilized in realizing the optimum SIW-to-microstrip transition without performing a parametric study by providing the characteristic end-termination impedances of an SIW structure. Furthermore, the proposed method addresses the challenging design of narrowband filters (i.e., FBW $< 5\%$) with insertion losses better than other reported efforts; thus, they are most suitable for applications that require narrowband channels and high stopband rejection. Finally, the proposed method can be integrated with other techniques to further enhance the overall electrical performance (i.e., introducing transmission zeros and achieving wide stopband characteristics for wideband BPFs).

APPENDIX

We first start at (7) and substitute λ_g and λ with $2\pi/\beta(\Delta x_m)$ and $1/(f\sqrt{\mu\varepsilon})$, respectively. Then (7) can be expressed as:

$$Z_{0,pi}(\Delta x_m) = k\frac{h}{w_{eff}(\Delta x_m)}\sqrt{\frac{\mu_r}{\varepsilon_r}}\frac{2\pi}{\beta(\Delta x_m)}f\sqrt{\mu\varepsilon} \quad \text{(A-1)}$$

which can be expressed in the following form:

$$Z_{0,pi}(\Delta x_m) = k\frac{h}{w_{eff}(\Delta x_m)}\frac{\omega\mu_r\sqrt{\mu_0\varepsilon_0}}{\beta(\Delta x_m)} \quad \text{(A-2)}$$

where $\omega = 2\pi f$. Then, the right-hand side is multiplied by the factor $(\varepsilon_0/\mu_0)^{1/2} \times (\mu_0/\varepsilon_0)^{1/2}$, leading to:

$$Z_{0,pi}\left(\Delta x_m\right) = \left(k\sqrt{\frac{\varepsilon_0}{\mu_0}}\right)\frac{h}{w_{eff}\left(\Delta x_m\right)}\frac{\omega\mu_r\sqrt{\mu_0\varepsilon_0}}{\beta\left(\Delta x_m\right)}\sqrt{\frac{\mu_0}{\varepsilon_0}} \tag{A-3}$$

Since $k(\varepsilon_0/\mu_0)^{1/2}$ is constant, it is denoted as k'. Then, (A-3) is written in the following form, considering that $\mu = \mu_0\mu_r$:

$$Z_0\left(\Delta x_m\right) = k'\frac{h}{w_{eff}\left(\Delta x_m\right)}\frac{\omega\mu}{\beta\left(\Delta x_m\right)} \tag{A-4}$$

Finally, provided that $Z_{wave}(\Delta x_m) = \omega\mu/\beta(\Delta x_m)$, (A-4) can be written as:

$$Z_0\left(\Delta x_m\right) = k'\frac{h}{w_{eff}\left(\Delta x_m\right)}Z_{wave}\left(\Delta x_m\right) \tag{A-5}$$

Q.E.D.

It is paramount to point out that the new constant, k', is a scaled version of k. Therefore, $k' = 1.2343$ is the value that matches $k = 465$ in the power-current definition given in (7).

REFERENCES

[1] S.-W. Wong, R. Sen Chen, K. Wang, Z.-N. Chen, and Q.-X. Chu, "U-shape slots structure on substrate integrated waveguide for 40-GHz bandpass filter using LTCC technology," *IEEE Trans. Compon., Packag., Manuf. Technol.*, vol. 5, no. 1, pp. 128–134, Jan. 2015.

[2] X.-P. Chen and K. Wu, "Self-packaged millimeter-wave substrate integrated waveguide filter with asymmetric frequency response," *IEEE Trans. Compon., Packag., Manuf. Technol.*, vol. 2, no. 5, pp. 775–782, May 2012.

[3] K. Wang, S.-W. Wong, G.-H. Sun, Z. N. Chen, L. Zhu, and Q.-X. Chu, "Synthesis method for substrate-integrated waveguide bandpass filter with even-order Chebyshev response," *IEEE Trans. Compon., Packag., Manuf. Technol.*, vol. 6, no. 1, pp. 126–135, Jan. 2016.

[4] S. W. Wong, K. Wang, Z.-N. Chen, and Q.-X. Chu, "Electric coupling structure of substrate integrated waveguide (SIW) for the application of 140-GHz bandpass filter on LTCC," *IEEE Trans. Compon., Packag., Manuf. Technol.*, vol. 4, no. 2, pp. 316–322, Feb. 2014.

[5] X.-P. Chen and K. Wu, "Substrate integrated waveguide filter: Basic design rules and fundamental structure features," *IEEE Microw. Mag.*, vol. 15, no. 5, pp. 108–116, Jul./Aug. 2014.

[6] D.-F. Guan, P. You, Q. Zhang, K. Xiao, and S.-W. Yong, "Hybrid spoof surface plasmon polariton and substrate integrated waveguide transmission line and its application in filter," *IEEE Trans. Microw. Theory Techn.*, vol. 65, no. 12, pp. 4925–4932, Dec. 2017.

[7] X. Chen, W. Hong, T. Cui, J. Chen, and K. Wu, "Substrate integrated waveguide (SIW) linear phase filter," *IEEE Microw. Wireless Compon. Lett.*, vol. 15, no. 11, pp. 787–789, Nov. 2005.

[8] K.-S. Chin, C.-C. Chang, C.-H. Chen, Z. Guo, D. Wang, and W. Che, "LTCC multilayered substrate-integrated waveguide filter with enhanced frequency selectivity for system-in-package applications," *IEEE Trans. Compon., Packag., Manuf. Technol.*, vol. 4, no. 4, pp. 664–672, Apr. 2014.

[9] A. R. Azad and A. Mohan, "Substrate integrated waveguide dual-band and wide-stopband bandpass filters," *IEEE Microw. Wireless Compon. Lett.*, vol. 28, no. 8, pp. 660–662, Aug. 2018.

[10] K. Zhou, C.-X. Zhou, and W. Wu, "Substrate-integrated waveguide dual-band filters with closely spaced passbands and flexibly allocated bandwidths," *IEEE Trans. Compon., Packag., Manuf. Technol.*, vol. 8, no. 3, pp. 465–472, Mar. 2018.

[11] R. Li, X. Tang, and F. Xiao, "Design of substrate integrated waveguide transversal filter with high selectivity," *IEEE Microw. Wireless Compon. Lett.*, vol. 20, no. 6, pp. 328–330, Jun. 2010.

[12] A. A. Khan and M. K. Mandal, "Narrowband substrate integrated waveguide bandpass filter with high selectivity," *IEEE Microw. Wireless Compon. Lett.*, vol. 28, no. 5, pp. 416–418, May 2018.

[13] W. Shen, W.-Y. Yin, X.-W. Sun, and L.-S. Wu, "Substrate-integrated waveguide bandpass filters with planar resonators for system-on-package," *IEEE Trans. Compon., Packag., Manuf. Technol.*, vol. 3, no. 2, pp. 253–261, Feb. 2013.

[14] L. Szydlowski, A. Jedrzejewski, and M. Mrozowski, "A trisection filter design with negative slope of frequency-dependent crosscoupling implemented in substrate integrated waveguide (SIW)," *IEEE Microw. Wireless Compon. Lett.*, vol. 23, no. 9, pp. 456–458, Sep. 2013.

[15] M. Le Coq, E. Rius, J.-F. Favennec, C. Quendo, B. Potelon, L. Estagerie, P. Moroni, B. Bonnet, and A. El Mostrah, "Miniaturized C-Band SIW filters using high-permittivity ceramic substrates," *IEEE Trans. Compon., Packag., Manuf. Technol.*, vol. 5, no. 5, pp. 620–626, May 2015.

[16] J. de Dios Ruiz, F. L. Martínez-Viviente, A. Alvarez-Melcon, and J. Hinojosa, "Substrate integrated waveguide (SIW) with Koch fractal electromagnetic bandgap structures (KFEBG) for bandpass filter design," *IEEE Microw. Wireless Compon. Lett.*, vol. 25, no. 3, pp. 160–162, Mar. 2015.

[17] W. Shen, "Extended-doublet half-mode substrate integrated waveguide bandpass filter with wide stopband," *IEEE Microw. Wireless Compon. Lett.*, vol. 28, no. 4, pp. 305–307, Apr. 2018.

[18] P. Li, H. Chu, and R.-S. Chen, "Design of compact bandpass filters using quarter-mode and eighth-mode SIW cavities," *IEEE Trans. Compon., Packag., Manuf. Technol.*, vol. 7, no. 6, pp. 956–963, Jun. 2017.

[19] Y. Cassivi, L. Perregrini, P. Arcioni, M. Bressan, K. Wu, and G. Conciauro, "Dispersion characteristics of substrate integrated rectangular waveguide," *IEEE Microw. Wireless Compon. Lett.*, vol. 12, no. 9, pp. 333–335, Sep. 2002.

[20] M. Bozzi, A. Georgiadis, and K. Wu, "Review of substrate-integrated waveguide circuits and antennas," *IET Microw., Antennas Propag.*, vol. 5, no. 8, pp. 909–920, Jun. 2011.

[21] A. Sahu, V. K. Devabhaktuni, R. K. Mishra, and P. H. Aaen, "Recent advances in theory and applications of substrate-integrated waveguides: A review," *Int. J. RF Microw. Comput.-Aided Eng.*, vol. 26, no. 2, pp. 129–145, Feb. 2016.

[22] F. Xu and K. Wu, "Guided-wave and leakage characteristics of substrate integrated waveguide," *IEEE Trans. Microw. Theory Techn.*, vol. 53, no. 1, pp. 66–73, Jan. 2005.

[23] K. A. Alshamaileh, V. K. Devabhaktuni, and N. I. Dib, "Impedance-varying broadband 90° branch-line coupler with arbitrary coupling levels and higher order harmonic suppression," *IEEE Trans. Compon., Packag., Manuf. Technol.*, vol. 5, no. 10, pp. 1507–1515, Oct. 2015.

[24] D. M. Pozar, *Microwave Engineering*, 4th ed. New York, NY, USA: Wiley, 2012.

[25] P. Rizzi, *Microwave Engineering: Passive Circuits*, 1st ed. Upper Saddle River, NJ, USA: Prentice-Hall, 1988.

[26] *ANSYS-High Frequency Structure Simulator (HFSS), Version 19.2*, ANSYS, Canonsburg, PA, USA, 2018.

[27] H. Ghorbaninejad and R. Heydarian, "New design of waveguide directional coupler using genetic algorithm," *IEEE Microw. Wireless Compon. Lett.*, vol. 26, no. 2, pp. 86–88, Feb. 2016.

[28] P. Kumar, A. Kedar, and A. K. Singh, "Design and development of low-cost low sidelobe level slotted waveguide antenna array in X-band," *IEEE Trans. Antennas Propag.*, vol. 63, no. 11, pp. 4723–4731, Nov. 2015.

[29] H.-C. Cheng, I.-C. Chung, and W.-H. Chen, "Thermal chip placement in MCMs using a novel hybrid optimization algorithm," *IEEE Trans. Compon., Packag., Manuf. Technol.*, vol. 2, no. 5, pp. 764–774, May 2012.

[30] J. Kim, T. Yoon, J. Kim, and J. Choi, "Design of an ultra wide-band printed monopole antenna using FDTD and genetic algorithm," *IEEE Microw. Wireless Compon. Lett.*, vol. 15, no. 6, pp. 395–397, Jun. 2005.

[31] R. Klopfenstein, "A transmission line taper of improved design," *Proc. IRE*, vol. 44, no. 1, pp. 31–35, Jan. 1956.

[32] K. A. Al Shamaileh, N. I. Dib, and A. Abbosh, "Analysis and design of ultra-wideband unequal-split Wilkinson power divider using tapered lines transformers," *Electromagnetics*, vol. 32, no. 7, pp. 426–437, Oct. 2012.

[33] C. T. Chiang and B.-K. Chung, "Ultra wideband power divider using tapered line," *Prog. Electromagn. Res.*, vol. 106, pp. 61–73, Jul. 2010.

[34] W. Hong, B. Liu, Y. Wang, Q. Lai, H. Tang, X. X. Yin, Y. D. Dong, Y. Zhang, and K. Wu, "Half mode substrate integrated waveguide: A new guided wave structure for microwave and millimeter wave application," in *Proc. Joint 31st Int. Conf. Infr. Millim. Waves 14th Int. Conf. Teraherz Electron.*, Shanghai, China, Sep. 2006, p. 219.

[35] Q. Lai, C. Fumeaux, W. Hong, and R. Vahldieck, "Characterization of the propagation properties of the half-mode substrate integrated waveguide," *IEEE Trans. Microw. Theory Techn.*, vol. 57, no. 8, pp. 1996–2004, Aug. 2009.
[36] B. Liu, W. Hong, Y.-Q. Wa, Q.-H. Lai, and K. Wu, "Half mode substrate integrated waveguide (HMSIW) 3-dB coupler," *IEEE Microw. Wireless Compon. Lett.*, vol. 17, no. 1, pp. 22–24, Jan. 2007.
[37] J.-X. Chen, Y. Zhan, W. Qin, Z.-H. Bao, and Q. Xue, "Novel narrow-band balanced bandpass filter using rectangular dielectric resonator," *IEEE Microw. Wireless Compon. Lett.*, vol. 25, no. 5, pp. 289–291, May 2015.

OSAMA I. HUSSEIN (Student Member, IEEE) received the B.Sc. degree in electrical engineering communications and electronics engineering from the Jordan University of Science and Technology (JUST), Jordan, in 2013. He is currently pursuing the "direct" Ph.D. degree in electrical engineering with The University of Toledo, USA. His research interests include microwave/millimeter wave components modeling and design, substrate integrated waveguide front-ends design, and applied optimization techniques to EM problems.

KHAIR A. AL SHAMAILEH (Member, IEEE) received the B.Sc. degree in telecommunications and electronics engineering and the M.Sc. degree in wireless communications engineering from the Jordan University of Science and Technology, Jordan, in 2009 and 2011, respectively, and the Ph.D. degree in engineering science, with an emphasis on electrical engineering, from The University of Toledo, OH, USA, in 2015. He is currently an Assistant Professor with the Electrical and Computer Engineering Department, Purdue University Northwest, Hammond campus. His interests include planar antenna design, microwave modeling, multi-/wideband passive and active RF/microwave components design, optimization techniques, wireless security and encryption, localization algorithms in wireless networks, mobile communications, and coding theory.

NIHAD I. DIB (Senior Member, IEEE) received the B.Sc. and M.Sc. degrees in electrical engineering from Kuwait University, in 1985 and 1987, respectively, and the Ph.D. degree in EE (major in electromagnetics and microwaves) from the University of Michigan, Ann Arbor, in 1992. Then, he was an Assistant Research Scientist with the Radiation Laboratory, University of Michigan. In September 1995, he joined the EE Department, Jordan University of Science and Technology (JUST) as an Assistant Professor, and became a Full Professor in August 2006. His research interests include computational electromagnetics, antennas, and modeling of planar microwave circuits.

AMIR NOSRATI received the B.Sc. degree in electrical and electronics engineering from the University of Razi, Kermanshah, Iran. He is currently pursuing the M.Sc. degree in communication engineering (field and wave) with the University of Tehran, Tehran, Iran. His current research includes the design and analysis of multi-band evanescent-mode substrate integrated waveguide bandpass filters.

SAID ABUSHAMLEH (Member, IEEE) received the B.Sc. degree in electrical and computer engineering from Hashemite University, Zarqa, Jordan, in 2007, the M.Sc. degree in wireless communications from Lund University, Lund, Sweden, in 2009, and the Ph.D. degree in telecommunications engineering from the University of Arkansas at Little Rock, Little Rock, Arkansas, in 2014. In 2015, he joined the Advanced Radar Research Center (ARRC), School of Meteorology, The University of Oklahoma, as a Postdoctoral Research Associate. Since August 2016, he has been with the Department of Physics and Astronomy: Engineering Foundations Program, The University of Nebraska at Kearney, Kearney, where he is currently an Assistant Professor of electrical engineering. His current research interests include antenna design for wearable electronics, microwave filters, and electromagnetic band gap structures and their applications in mutual coupling reduction among antenna elements. He is a member of the Jordan Engineers Association (JEA).

DANIEL G. GEORGIEV (Senior Member, IEEE) received the M.S. degree in engineering physics from Sofia University, Bulgaria, in 1994, and the Ph.D. degree in electrical engineering from the University of Cincinnati, OH, USA, in 2003. In 2006, he joined The University of Toledo, where he is currently an Associate Professor and serves as the Graduate Program Director for the Department of Electrical Engineering and Computer Science. His research interests include electronic materials and devices, laser processing of materials, photovoltaics, and semiconducting glassy materials.

VIJAY KUMAR DEVABHAKTUNI (Senior Member, IEEE) received the B.Eng. degree in electrical and electronics engineering and the M.Sc. degree in physics from the Birla Institute of Technology and Science, Pilani, India, in 1996, and the Ph.D. degree in electronics from Carleton University, Ottawa, Canada, in 2003. He held the competitive Natural Sciences and Engineering Research Council of Canada (NSERC) Postdoctoral Fellowship and spent the tenure researching with Dr. J.W. Haslett at the University of Calgary, Calgary, Canada, from 2003 to 2004. In 2005, he taught at Penn State Behrend. From 2005 to 2008, he held the Canada Research Chair in computer-aided high-frequency modeling and design with Concordia University, Montreal, Canada. In 2008, he joined the Department of Electrical Engineering and Computer Science, The University of Toledo, Toledo, as an Associate Professor, and was promoted to a Professor in 2013. In 2018, he joined Purdue University Northwest, Hammond, as a Chair of the Department of Electrical and Computer Engineering. He secured external funding close to $5M in his research areas (sponsoring agencies include AFOSR, AFRL, CFI, NASA, NIST, NSERC, NSF, ONR, and industry partners). He authored 250 peer reviewed articles. His interests include applied electromagnetics, the biomedical applications of wireless sensor networks, computer aided design, device modeling, image processing, infrastructure monitoring, neural networks, RF/microwave design, unmanned aerial vehicles (UAVs), and virtual reality. In Canada and USA, he graduated 75 theses students at M.S. and Ph.D. levels and received student nominated teaching excellence awards. He served as the Associate Editor for the *International Journal of RF and Microwave Computer-Aided Engineering* under Editor-in-Chief Dr. Inder Bahl. He is a Professional Engineer of the Association of Professional Engineers and Geoscientists of Alberta (APEGA).